PNAS RESEARCH ARTICLE | PHYSICS

Nanocolloidal hydrogel mimics the structure and nonlinear mechanical properties of biological fibrous networks

Elisabeth Prince[a,b,c], Sofia Morozova[a,d], Zhengkun Chen[a], Vahid Adibnia[a,e], Ilya Yakavets[a], Sergey Panyukov[f,g], Michael Rubinstein[h,i,j,k,l,1], and Eugenia Kumacheva[a,m,n,1]

Edited by Frederick C. MacKintosh, Rice University, Houston, TX; received December 6, 2022; accepted October 3, 2023 by Editorial Board Member Paul Chaikin

Fibrous networks formed by biological polymers such as collagen or fibrin exhibit nonlinear mechanical behavior. They undergo strong stiffening in response to weak shear and elongational strains, but soften under compressional strain, in striking difference with the response to the deformation of flexible-strand networks formed by molecules. The nonlinear properties of fibrous networks are attributed to the mechanical asymmetry of the constituent filaments, for which a stretching modulus is significantly larger than the bending modulus. Studies of the nonlinear mechanical behavior are generally performed on hydrogels formed by biological polymers, which offers limited control over network architecture. Here, we report an engineered covalently cross-linked nanofibrillar hydrogel derived from cellulose nanocrystals and gelatin. The variation in hydrogel composition provided a broad-range change in its shear modulus. The hydrogel exhibited both shear-stiffening and compression-induced softening, in agreement with the predictions of the affine model. The threshold nonlinear stress and strain were universal for the hydrogels with different compositions, which suggested that nonlinear mechanical properties are general for networks formed by rigid filaments. The experimental results were in agreement with an affine model describing deformation of the network formed by rigid filaments. Our results lend insight into the structural features that govern the nonlinear biomechanics of fibrous networks and provide a platform for future studies of the biological impact of nonlinear mechanical properties.

hydrogels | fibers | mechanical properties

Networks formed by protein fibers are ubiquitous in biological systems. The cellular cytoskeleton is composed of actin fibers, microtubules, and intermediate filaments (1). The extracellular matrix (ECM) contains collagen, elastin, and fibronectin fibers (2). The scaffold of blood clots is a gel formed by a branching network of fibrin fibers (3). The stiff nature of the constituent fibers impacts many biological processes, including cell migration, intracellular communication, tumor formation, and pathological conditions such as fibrosis (4–7).

The fibrillar network architecture imparts biological materials with distinct mechanical properties (8). It is established that networks of fibrin, collagen, and actin display strong nonlinear stiffening; that is, a small (<10%) increase in shear or elongational strain leads to a more than 10-fold increase in gel stiffness (8–12). Such response to deformation allows soft and compliant biomaterials to stiffen and resist rupture when exposed to strains that may otherwise threaten tissue integrity (3, 8, 13, 14). The nonlinear strain-stiffening of fibrillar networks also impacts the local mechanical microenvironment sensed by cells and facilitates long-distance cell-to-cell communication through fiber alignment and mechanical forces propagating through the extracellular matrix (15–17). Another unique feature of biological fibrillar networks, including fibrin, collagen, and actin, is their mechanical asymmetry: While stiffening occurs in response to shear and extensional strain, compressional strain results in the decrease of the shear modulus (18–20). Mechanical asymmetry may have implications in mechanobiology, as cell proliferation in tumors and other systems impose compressive strain on the surrounding fibrillar ECM, thus, altering its stiffness(21).

Both of these nonlinear mechanical properties of biological filamentous gels are attributed to the mechanical asymmetry of the constituent protein fibers that have a bending modulus significantly smaller than their stretching modulus (12, 19), although local deformations are another important factor in the behavior of extracellular matrices made of collagen (22). Stretching of protein fibers is resisted by the strong intrafiber covalent and noncovalent interactions (3, 8, 10). In contrast, networks formed by crosslinking flexible molecules and strands are highly extensible and at the low strains, do not exhibit asymmetric force-extension relationship.

Significance

Advancements in tissue engineering are limited by reliance on contrived hydrogels that fail to mimic the native nanofibrillar architecture and mechanical properties of biological tissues. We report a biomimetic hydrogel that addresses this challenge by recapitulating the filamentous structure and the unique mechanical behavior of the fibrous protein networks. The hydrogel exhibited shear-stiffening and compression-induced softening, in agreement with the predictions of the developed affine model for athermal bent network. The nonlinear mechanical behavior of the hydrogel was attributed to the mechanical asymmetry of the constituent filaments. The variation in hydrogel composition offered a way to control its mechanical properties. Our results show that the nonlinear mechanical properties of biological fibrous gels can be recapitulated in engineered fibrillar hydrogels.

Competing interest statement: E.P. and E.K. have filed an International PCT patent application related to this work (Serial No. PCT/CA2018/050862, Filing Date: July 16, 2018).

This article is a PNAS Direct Submission. F.C.M. is a guest editor invited by the Editorial Board.

[1]To whom correspondence may be addressed. Email: mr351@duke.edu or eugenia.kumacheva@utoronto.ca.

This article contains supporting information online at https://www.pnas.org/lookup/suppl/doi:10.1073/pnas.2220755120/-/DCSupplemental.

Published December 13, 2023.

Studies of the nonlinear mechanical properties of fibrillar networks have primarily been limited to biological fibrillar hydrogels (3, 8, 9, 23–26). Engineered hydrogels mimicking the fibrillar biological networks would enable synthetically controlled variation in their mechanical behavior and offer the capability to perform fundamental studies of filamentous networks. Currently, however, it is not established whether nonlinear strain-stiffening and mechanical asymmetry are the universal properties of all—biological and synthetic—fibrillar hydrogels.

Synthetic hydrogels formed by cross-linked polymer molecules, e.g., polyacrylamide or poly(ethylene glycol), lack a fibrillar architecture. Due to the inherent extensibility of the flexible polymer chains (8, 27–30), "molecular" hydrogels exhibited linear elastic behavior up to high (100 to 400%) strains and, therefore, fail to recapitulate the nonlinear properties of rigid filamentous networks (31, 32). Synthetic fibrillar hydrogels recapitulating the architecture of biological filamentous hydrogels have been derived from shape-anisotropic nanoparticles (33–36), amphiphilic peptides (37, 38), and block-copolymer micelles (39, 40). Studies of engineered hydrogels recapitulating the mechanical properties of biological fiber networks have been limited to hydrogels formed from bottlebrush polymers (41, 42) and polyisocyanopeptide bundles (43, 44), which exhibited both nonlinear strain-stiffening and mechanical asymmetry.

Here, we recapitulate the nonlinear mechanical behavior of biological fibrillar hydrogels in an engineered hydrogel formed by rod-shaped cellulose nanocrystals. These gels have a filamentous architecture that mimics the structure of protein networks (32, 34–36); however, their nonlinear response to deformation has not been studied. A fibrous hydrogel (later in the text, referred to as EKGel) was synthesized by cross-linking gelatin and aldehyde-modified cellulose nanocrystals (aCNCs). We show that at a physiological temperature of 37 °C, the EKGel displays the composition-dependent nonlinear strain-stiffening behavior, thus, replicating the response to the deformation of fibrous collagen and fibrin networks. Furthermore, similar to fibrous protein networks, EKGel exhibited mechanical asymmetry, that is, compression-induced softening and stretching-mediated stiffening. Our results suggest that the nonlinear mechanical properties of biological tissues can be recapitulated in engineered fibrous gels formed by sufficiently long and stiff fibers. In our earlier work, it has been established that EKGel is biocompatible and does not disrupt the gene expression, proliferation, or drug response of patient-derived cancer (35, 45–47). Thus, this gel can serve as a platform for mechanobiology studies to elucidate the impact of nonlinear mechanics in biological processes.

Theoretical Model

To explain and predict the nonlinear mechanical behavior of fibrillar hydrogels, we use an affine model for the network formed by rigid filaments, which are defined as fragments of fibers connecting two neighboring cross-linking points in the network (48). The network of athermal filaments with the effective coordination number $\boldsymbol{Z} \leq 2\mathrm{d}$ (=6 for d = 3 dimensional network) would be flexible with zero shear modulus (49). This criterion of flexibility for $Z < 2\mathrm{d}$ is applicable only for freely jointed filaments with two cross-links per filament that forms a single fiber. In our work (as we show below), the observed finite shear modulus at small strains is due to the fact that on average, the fibers have more than two cross-links per fiber, and thus, the fibers consist of multiple filaments. For this reason, the filaments between the cross-links are not freely jointed, as two neighboring filaments often belong to the same fiber. Therefore, we consider a typical fiber with more than two cross-links as having a large number of constraints that are responsible for the nonzero shear modulus of the network (as if $\boldsymbol{Z} > 6$). On mesoscopic scales, all such networks deform affinely. Since in our work fibers are multiply cross-linked, we assume that the affine length scale (which is the smallest scale of affine deformation) is on the order of the size of an elementary cell of the network. In our model, we replaced the network of multiply connected fibers consisting of several bent filaments with the affine model of these filaments. This model was introduced for biaxially compressed fibrin networks in our previous work (48); however, we admit that it can fail to describe strongly irregular structure with high polydispersity of filament lengths.

We start from an undeformed gel with randomly oriented fibers and impose either sole shear or shear combined with uniaxial compression or extension in the orthogonal direction. By minimizing the total elastic energy of the network, we predict fiber dimensions, fiber orientation distribution, and the stress in the deformed gel. The details of the theoretical model are provided in *SI Appendix*.

The elasticity of enthalpic gels arises from bending of the constituent filaments. The values of the bending and stretching moduli of the filaments, k_b and k_s, respectively, can be found from their structural characteristics. Fig. 1*A* shows a filament with its characteristic dimensions, that is, diameter (d), length between junctions (L, contour length), the end-to-end distance (R), deflection P, and arc angle, Ψ. The rigid filaments are considered to be enthalpic springs with bending and stretching moduli

$$k_b = \frac{9\pi E d^4}{4\Psi^2 L}, \qquad [1]$$

$$k_s = \frac{\pi E d^2 L}{4}, \qquad [2]$$

where E is the Young modulus of the filament. In enthalpic filamentous networks, such as collagen and fibrin, the fibers are significantly stiffer upon stretching than upon bending (49, 50), that is, they exhibit the force-extension asymmetry with $k_s/k_b \sim (L\Psi/d)^2 \gg 1$.

Fig. 1*B* shows an undeformed gel with initial thickness h_i and randomly oriented filaments. Under the shear strain, γ, these filaments bend and stretch, as shown in Fig. 1*C*, while the gel thickness remains h_i. In the sheared gel, there is a direction of maximum extension of the gel, while in the orthogonal direction, the gel is compressed. When the shear strain is smaller than the cross-over value ($\gamma < \gamma_s \approx \Psi^2/12$), the stress–strain relationship for the gel is reflected by the linear shear elastic modulus

$$G \simeq \frac{\sigma}{\gamma} \simeq \nu k_b, \qquad [3]$$

which is proportional to the bending modulus of the filaments, k_b, and their number density ν in the undeformed gel (*SI Appendix*).

For the stronger shear stress, $\sigma > \sigma_s = G\gamma_s$, the filaments that are oriented mainly along the axis of maximum deformation are straightened out. Further filament deformation is small and is described by their stretching modulus, $k_s (\gg k_b)$. The filaments oriented in the compression direction are still bent. With a further increase in σ the fraction $\phi_s \approx \sigma / \left(\nu k_s \gamma_c\right)$ of strongly stretched filaments increases (*SI Appendix*), and finally, at $\sigma > \sigma_c = G\gamma_c \left(\gamma_c > \gamma_s\right)$, these filaments form a rigid subnetwork which only slightly deforms ($\gamma \approx \gamma_c$) with increasing σ. In this regime, the differential modulus of the network:

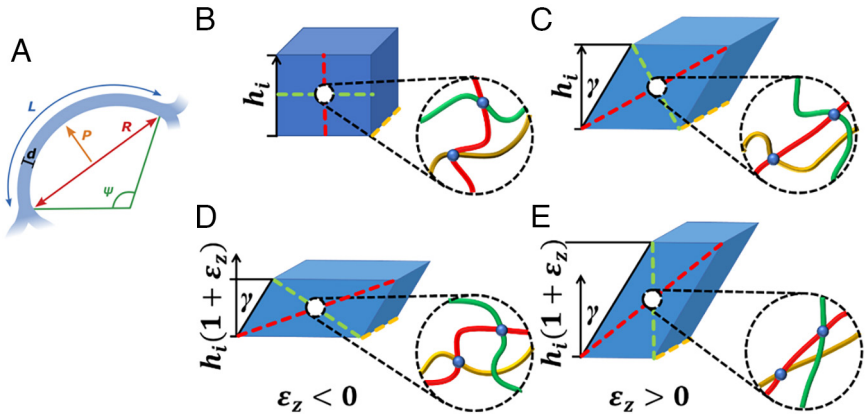

Fig. 1. Illustration of deformation of rigid-filament gel with original thickness h_i. (*A*) Structural characteristics of the filaments, including their contour length, *L*, end-to-end distance, *R*, diameter, *d*, deflection *P*, and arc angle, Ψ. Schematics of undeformed gel (*B*); sheared gel (*C*); simultaneously sheared and compressed in z-direction gel (*D*) and simultaneously sheared and stretched in z-direction gel (*E*). *Insets* show the corresponding deformation of oriented fibers.

$$K' = \frac{d\sigma}{d\gamma} \approx \phi_s \nu k_s \approx \frac{\sigma}{\gamma_c}, \qquad [4]$$

is proportional to the fraction ϕ_s of the highly stretched filaments and their stretching modulus k_s, which is significantly higher than their bending modulus k_b.

Simultaneous shear and compression of the fibrous gel is illustrated in Fig. 1*D*. Compression is quantified by strain $\varepsilon_z = (h - h_i)/h_i < 0$, where h is the gel thickness after deformation. Compression of the shear-strained gel reduces the extension of the filaments oriented along the axis of maximum gel stretching and reduces the shear storage modulus of the compressed gel, in comparison with G. By contrast, concurrent shear and stretching of the gel in the z-direction by the factor $\varepsilon_z = (h - h_i)/h_i > 0$ (Fig. 1*E*) leads to an increase in the fraction ϕ_s of strongly stretched filaments and, as a result, an increase in its shear modulus, in comparison with G.

Experimental Results

Fig. 2*A* illustrates the hierarchical structure of EKGel formed by gelatin and cellulose nanocrystals modified with aldehyde groups (aCNCs). The aCNCs had an average diameter and length of 14.4 ± 3.7 and 141 ± 36 nm, respectively (*SI Appendix*, section S1), while the estimated radius of gyration of gelatin with the weight average molecular weight of 70, 000 kDa was 17 nm (51, 52). The EKGel was formed in a buffered salt solution (Hank's Balanced Salt Solution, HBSS) in a two-step process. First, aCNCs assembled into a fibrous network, due to a high ionic strength of HBSS, which resulted in suppressed electrostatic repulsion between the charged aCNCs and hence, their association (34). Second, gelatin adsorbed to aCNCs and chemically cross-linked them within the fibers by forming covalent imine cross-links between the aldehyde groups of aCNCs and primary amino groups of gelatin (Fig. 2*A*). Since EKGel has biomedical applications (45–47, 53), all further experiments were performed at 37 °C, unless otherwise specified. Fig. 2 *B* and *C* shows representative scanning electron microscopy (SEM) images of EKGel with different total concentrations of hydrogel components, $C_{total} = C_{aCNC} + C_{gel}$. Analysis of these images revealed that the average fiber diameters did not significantly change, when C_{total} was increased from 1.0 to 5.0 wt%, respectively, thus, indicating that, on average, two to three aCNCs were packed side-by-side within the fibers. Furthermore, the average filament length (the average fiber fragments between the two junctions) varied from approximately 480 to 379 nm with C_{total} increasing from 1.0 to 5.0 wt%, respectively, suggesting that, on average, filaments contained three to six aCNCs in length.

To confirm that aCNCs and gelatin are colocalized in the fibers, as shown in Fig. 2*A*, these EKGel components were covalently labeled with rhodamine-B isothiocyanate (RBITC) and CF-488A fluorescent dyes, respectively, which emitted in the green and red spectral range. Imaging of EKGel by confocal fluorescence microscopy revealed that gelatin and aCNCs were colocalized within the fibers (*SI Appendix*, Fig. S2). The colocalization of aCNCs and gelatin was quantified by calculating the Pearson Correlation Coefficient (PCC), which characterizes the overlap of two channels in fluorescence microscopy (54). Fig. 2*D* shows the PCC values for EKGels with different aCNC concentrations, C_{aCNC}, and gelatin concentrations, C_{gel}, of 2.0 wt%. For EKGel with all compositions, the PCC was significantly larger than the threshold value of 0.3 (54), which indicated the colocalization of aCNCs and gelatin in the composite fibers.

The formation of imine cross-links between the aldehyde groups on the aCNC surface and the primary amine groups gelatin in EKGel was quantified by first measuring the concentration of aldehyde groups on the aCNC surface as reported elsewhere (55, 56) and TNBS assay to determine the consumption of the amino groups of gelatin (*SI Appendix*, Fig. S3). The concentration of aldehyde groups per gram of aCNCs was 906 μmol/g, and the concentration of amine groups per gram of gelatin was 213 μmol/g. Within EKGel, the mass ratio of aCNCs-to-gelatin was 1:1.

Based on the analysis of SEM images of EKGel, we determined the structural characteristics of the filaments, that is, diameter (d), length between junctions (L, contour length), the end-to-end distance (R), and arc angle (Ψ) (Fig. 1*E* and *SI Appendix*, Fig. S4). We note that SEM images represent a two-dimensional projection of the 3D filament network, and thus, we measured the 2D projections of R and L onto the x-y plane, r and l, respectively. Both R and L values were calculated from their 2D projections, as described in *SI Appendix*, section S3. The curvature of the filaments was characterized by the arc angle, Ψ, as illustrated in Fig. 1*A*, which was calculated from R, L, and d values.

Table 1 lists the average values of d, L, and Ψ for EKGel with different compositions. Increasing C_{total} from 1.0 to 5.0 wt%, while maintaining the ratio $C_{aCNC}/C_{gel} = 1.0$ resulted in smaller L values and insignificant change in d (one-way ANOVA test, $P = 0.4$). We note that at all C_{total} values, the fiber diameters were larger than the diameter of individual aCNCs of 14 ± 4 nm, suggesting that fibers consisted of multiple aCNCs across.

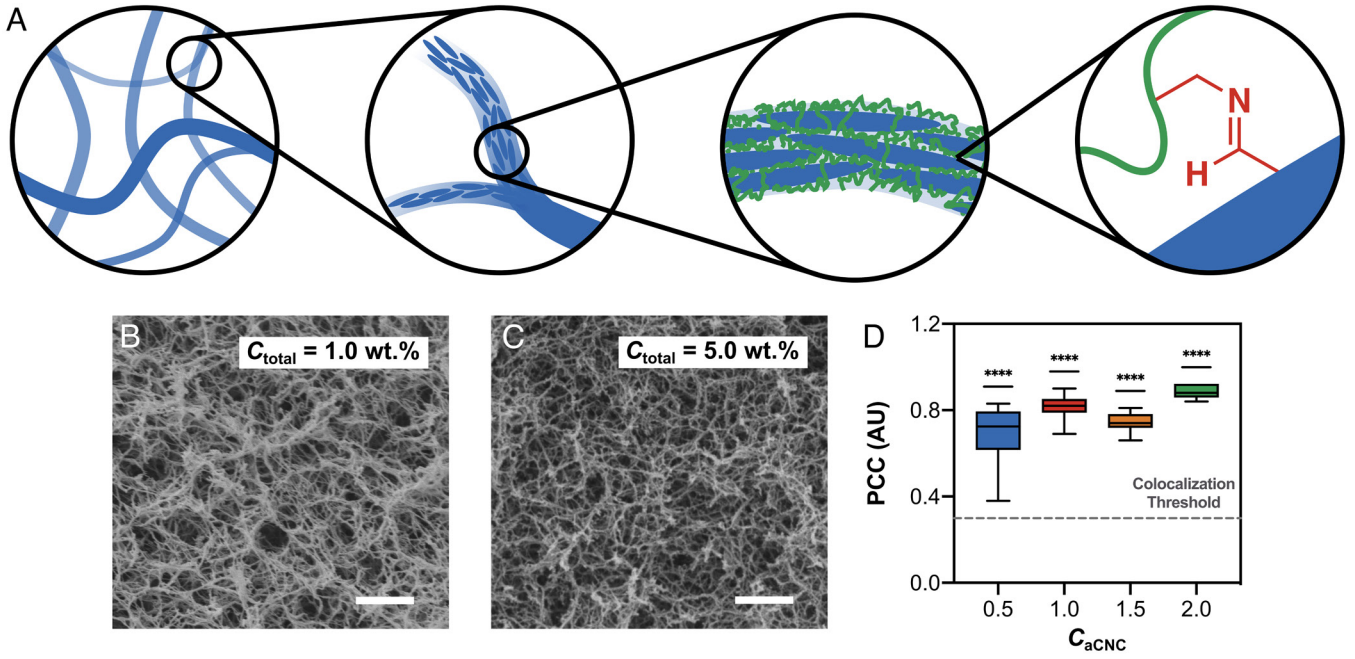

Fig. 2. Structure of EKGel. (*A*) Schematics of the hierarchical EKGel structure of the network (left cartoon), cross-section of individual fibers (middle cartoons), and the molecular level (right cartoon). (*B* and *C*) SEM image of EKGel with C_{total} = 1.0 wt% (*B*) and C_{total} = 5.0 wt% (*C*). In (*B* and *C*), C_{aCNC}/C_{gel}=1.0. Scale bars are 1 μm. (*D*) Pearson colocalization coefficient (PCC) of gelatin and aCNCs in EKGels with different C_{aCNC} and constant C_{gel}= 2.0 wt%. Boxes indicate mean SD, with whiskers indicating the minimum and maximum values. Analysis was performed on N = 11 images of different gel regions. One gel was imaged for each C_{aCNC}. The dashed line at PCC = 0.3 indicates the threshold for colocalization of aCNCs and gelatin. ****P < 0.0001, one-sample t test, hypothetical mean is 0.3.

We also characterized the porosity of EKGel by measuring the mesh size, ξ, or the average distance between filaments. Since the value of ξ measured from SEM images is an underestimation of the pore size, as the SEM images are a 2D projection of a 3D network, we determined ξ by measuring Darcy's permeability of EKGel (28, 48, 49), as shown in *SI Appendix*, Fig. S5. Table 1 shows that with C_{total} increasing from 1.0 to 5.0 wt% at C_{aCNC}/C_{gel} = 1.0, the value of ξ decreased from 730 to 190 nm (one-way ANOVA test, P = 0.0096, N = 3). For comparison, the corresponding values of ξ measured from the SEM images ranged from 409 ± 15 to 88 ± 5 nm (*SI Appendix*, Fig. S5 and Table S2). Notably, the values of ξ from permeability measurements closely followed the predicted relationship $\xi \sim \langle d \rangle / \sqrt{\phi}$, where $\langle d \rangle$ is the average fiber diameter and ϕ is the volume fraction of fibers (*SI Appendix*, Fig. S6) (57–59). To summarize, a denser network with smaller pores and less curved filaments was formed in EKGel with increasing C_{total}.

Table 2 lists k_b, k_s, and the ratio k_s / k_b for EKGel with different C_{total}, which were determined using Eqs. **1** and **2** (the determination of the value of E is described in *SI Appendix*, section S4). Similar to collagen, fibrin, and other biological fibrillar networks with rigid fibers, EKGel's fibers exhibited $k_s / k_b \gg 1$ at all C_{total} values. Based on the EKGel composition and structure (Fig. 2*A*), we expect the Young's modulus of the fibers to be intermediate between the CNC and gelatin gel moduli.

As there are four types of networks, that is, i) thermal semiflexible (49, 60), ii) thermal flexible (61, 62), iii) athermal straight (63, 64), and iv) athermal bent (48) networks, based on our experimental observations, in the present work, we excluded from the consideration the networks with thermal flexible and athermal straight filaments and compared the remaining networks composed of thermal semiflexible and athermal bent filaments.

In *SI Appendix*, section S4, we considered the enthalpic and entropic mechanisms of EKGel's elasticity. We first assumed that EKGel's elasticity follows the entropic mechanism and using the measured value of the shear modulus of EKGel, calculated the thermally induced bending angle of the filaments. We found that this angle would be an order of magnitude smaller than the experimentally measured angle (*SI Appendix*, Table S3). Thus, we concluded that the curvature of the filaments is intrinsic and is not determined by thermal fluctuations. We next considered the enthalpic mechanism of EKGel's elasticity and estimated the persistence length of filaments. We found it to be on the order of hundreds of micrometers (*SI Appendix*, Table S4), that is, many

Table 1. Structural characteristics of EKGel

C_{total}	d, nm*	L, μm†	Ψ†	ξ, nm‡
1.0 wt%	27 ± 7	0.460	1.92	728 ± 16
3.0 wt%	28 ± 8	0.409	1.85	384 ± 98
5.0 wt%	29 ± 12	0.404	1.39	189 ± 51

*Determined from SEM images and shown as mean ± SD (N = 110, 73, and 107 for C_{total} = 1.0, 3.0, and 5.0 wt%, respectively.
†Calculations of L and Ψ are provided in *SI Appendix*, section S3.
‡Determined from the Darcy permeability (*SI Appendix*, section S3). Data shown as mean ± SEM, N = 3.

Table 2. Mechanical properties of EKGel filaments

C_{total}, wt%	k_b(fJ)*	k_s (fJ)†	k_s / k_b
1.0	0.050	5.73	114.5
3.0	0.043	3.53	81.7
5.0	0.040	1.64	41.0

*Determined with Eq. **1** and values included in Table 1.
†Determined with Eq. **2** and values included in Table 1.

orders of magnitude larger than the filament length of 380 to 480 nm, which indicated that thermal fluctuations are not significant for the observed curvature of the filaments and EKGel's mechanical properties. Since the comparison of the experimentally observed curvature of the filaments in the EKGel was inconsistent with thermally induced curvature, we concluded that EKGel belongs to the athermal bent class of networks, and other models (49, 60–64) do not describe its architecture and mechanical properties. For this athermal bent class of networks, we used the affine model developed by our group (48), which was in agreement with experimental results.

With an assumption that the bending vs. stretching asymmetry of EKGel's fibers would impart the gel with the same nonlinear strain stiffening as that of biological networks with stiff fibers, we experimentally studied the strain stiffening of EKGel. The nonlinear stiffening of EKGel was characterized by measuring the differential modulus $K' = d\sigma/d\gamma$, where σ and γ are the shear stress and strain, respectively. Experiments were conducted using the established prestress protocol for determining K', where small oscillatory shear strains are applied under prestress, that is, the stress was increased to a constant applied value, and the small oscillations were performed around that stress (43, 61). Fig. 3 *A* and *B* shows that in the stress range $1.0 \le \sigma \le 60$ Pa (Fig. 3*A*) and strain range $0.002 \le \gamma \le 0.15$ (Fig. 3*B*), the value of K' was approximately 400 Pa; however, above a critical shear stress, σ_c, of 66 Pa and critical shear strain, γ_c, of 0.15, the value of K' increased from 414 to 2,650 Pa, with σ and γ increasing to 600 Pa and 0.22, respectively. In these experiments, the value of σ_c was determined by normalizing K'/G and extrapolating the variation of K' vs. σ in the high stress region to $K'/G = 1.0$. The critical strain, γ_c, was determined as $\gamma_c = \sigma_c/G$. Thus, a sixfold increase in the value of K' was observed when γ/γ_c increased from 1.0 to 1.5.

The variations of K' vs. σ and K' vs. γ for EKGel were compared with similar characteristics of biological fibrillar networks (Fig. 3). In the experiments, above σ_c and $\gamma_c \approx \sigma_c/G$, fibrin and collagen I gels exhibited a more than 10-fold increase in K', when γ/γ_c, reached 3.3 and 5.3, respectively, thus, exhibiting nonlinear strain-stiffening, in agreement with earlier reports (8). The value of σ_c was 0.5, 20, and 66 Pa for collagen I, fibrin, and EKGel (C_{total} = 5.0 wt%, C_{aCNC}/C_{gel} = 1.0), respectively (Fig. 3*A*). The value of γ_c was 0.008, 0.05, and 0.15 for collagen I, fibrin, and EKGel (C_{total} = 5.0 wt%, C_{aCNC}/C_{gel} = 1.0), respectively (Fig. 3*B*). For comparison, in Fig. 3 *A* and *B* we also show the variation of K' vs. σ and K' vs. γ, respectively, for polyacrylamide gel formed by flexible polymer chains. In the entire range of σ and γ values studied; this gel did not display nonlinear strain-stiffening.

Notably, the presence of gelatin and intrafiber imine cross-links was critical for EKGel to display nonlinear strain-stiffening behavior. A hydrogel formed by aCNCs in HBSS buffer (in the absence of gelatin), did not exhibit strain-stiffening (*SI Appendix*, Fig. S7). Instead, this gel disassociated and broke at $\sigma = 30$ Pa, due to the weak physical bonding of aCNCs. The ability to modulate nonlinear strain-stiffening was explored by varying hydrogel composition, that is, C_{total}, C_{aCNC}, and C_{gel}. Fig. 4 *A*–*C* show that increasing C_{total} resulted in higher G, σ_c, and γ_c. This result was in agreement with Eqs. **3** and 4 that predict an increase in G, σ_c, and γ_c, due to an increase of the ratio k_b/k_s and fiber density (Tables 1 and 2) with C_{total}. The variation in G, σ_c, and γ_c showed the same dependence on both C_{total} and C_{aCNC} (the latter shown in *SI Appendix*, Fig. S8). Notably, the nonlinear strain-stiffening dependence was reproducible for replicated EKGel samples with the same C_{total} (*SI Appendix*, Fig. S9).

We note that the stresses exerted by cells on their fibrous ECM and the stress exerted on fibrin blood clots within arteries are in the range of 1 to 100 Pa. This biologically relevant range of stresses was explored in our work and is shaded in Fig. 4*C*. Importantly, all EKGels examined in our work exhibited σ_c from 1.8 to 69 Pa, and therefore, they may exhibit nonlinear strain-stiffening in response to biologically relevant stresses. The values of γ_c for EKGel with different C_{total} changed from 0.11 to 0.22. Notably, according to Eq. **3**, the value of γ_c depends on fiber stiffness (k_b and k_s), L, and the fiber density (υ), which is related to the mesh size (ξ). These parameters depend differently on C_{total}, that is, k_b and k_s (Table 1) and L (Table 2) decrease with increasing C_{total}, while υ increases at larger C_{total}, as reflected by the decrease in ξ (Table 1). The difference in the effect of C_{total} on the structural characteristics of EKGel may account for the nonmonotonic dependence of γ_c vs. C_{total} (Fig. 4*C*). Furthermore, when C_{total} increased from 1.0 to 5.0 wt%, the maximum stress before rupture varied from 30 to 600 Pa, respectively.

In contrast, at 37 °C the values of K' and σ_c remained constant when C_{gel} changed from 0.5 to 4.0 wt% (Fig. 4*D*). We note that since the sol–gel transition for gelatin is in the range of 20 to 30 °C (61, 62), at 37 °C gelatin is in a liquid (molecular) state,

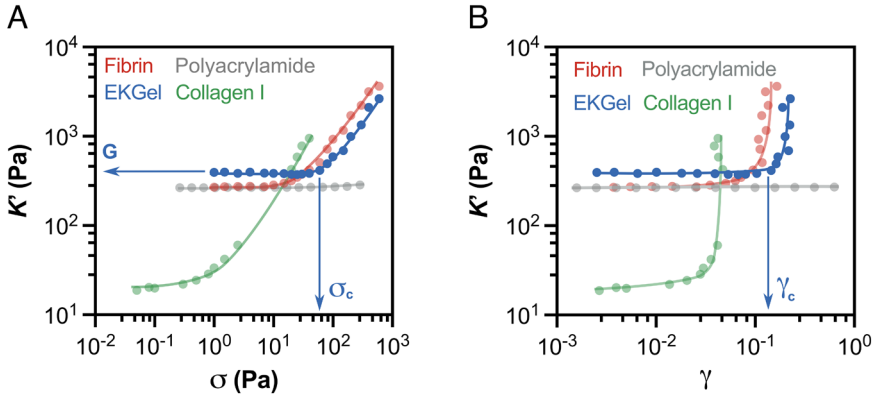

Fig. 3. Nonlinear strain-stiffening. (*A* and *B*) Variation in differential modulus, K', with shear stress (*A*) and shear strain (*B*) for fibrin gel (red), collagen I gel (green), polyacrylamide gel (gray), and EKGel (blue). Fibrin gel: bovine fibrin and thrombin concentrations were 22.8 mg/mL and 5 U/mL, respectively, in tris-buffered saline with 3 mM $CaCl_2$. Collagen gel: Collagen I from rat tail was 2 mg/mL in 1X HBSS. Polyacrylamide: acrylamide and the *bis*-acrylamide cross-linker concentrations were 3 wt% and 0.16 wt%, respectively. In EKGel, C_{total} = 5.0 wt% (C_{aCNC} = C_{gel} = 2.5 wt%). (*A*) Blue arrows indicate the modulus, G, and the critical stress, σ_c, corresponding to the beginning of EKGel stiffening. (*B*) Blue arrow indicates the critical strain, γ_c, corresponding to the onset of EKGel stiffening. Lines are for eye guidance. The maximal stress corresponds to the highest stress measured before hydrogel rupture. The initial shear stress was 1.0 Pa for fibrin gel and EKGel, 0.05 Pa for collagen gel, and 0.3 Pa for polyacrylamide gel.

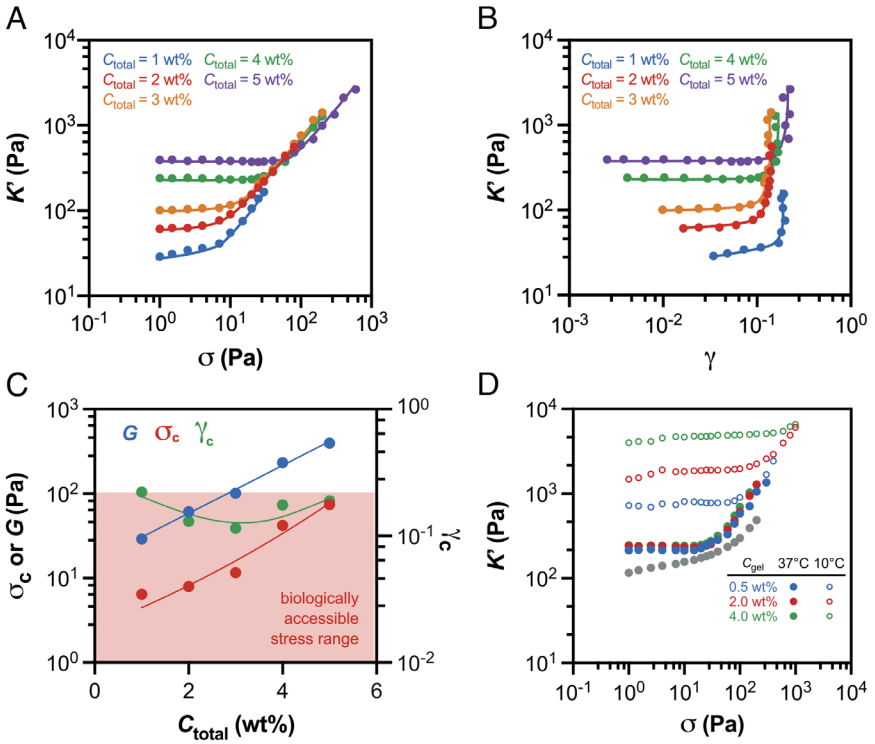

Fig. 4. Compositional control over nonlinear strain-stiffening of EKGel. (*A* and *B*) Variation in K' with σ (*A*) and γ (*B*) with varying C_{total}. (*C*) Effect of C_{total} on σ_c, γ_c, and G'. In (*A* and *B*), T = 37 °C. (*D*) Variation in K' vs. σ with varying C_{gel} at 10 °C (open symbols) and 37 °C (filled symbols). C_{aCNC} = 2.0 wt%. The gray circles in (*D*) correspond to the 2.0 wt% gelatin gel at 10 °C. In (*A*–*C*), C_{aCNC}/C_{gel} = 1.0 and T = 37 °C. Lines are for eye guidance. The maximal stress corresponds to the highest stress measured before hydrogel rupture. The initial shear stress was 1 Pa.

that is, at the amount incorporated in EKGel, gelatin did not form a network (*SI Appendix*, Fig. S10). Therefore, at 37 °C, the CNCs in the composite fibers were permanently cross-linked by individual gelatin molecules (acting as soft springs between the neighboring CNCs), which caused invariance in the K' and σ_c values. When the hydrogel temperature was reduced to 10 °C, the EKGel exhibited strain stiffening that was affected by C_{gel}, that is, the values of G and σ_c increased with higher C_{gel} (Fig. 4*D*). At this temperature, gelatin formed a gel between the CNCs in the fibers, that is, the neighboring CNCs become connected by the stiffer springs of the gelatin network. Therefore, the composite fibers have a higher shear modulus. Because of the difference in the fiber moduli, in the nonlinear regime, the dependence of K' on stress started at higher values of σ for the EKGel at a lower temperature. Notably, a 2.0 wt% gelatin gel (in the absence of aCNCs) exhibited strain stiffening at 10 °C, presumably, due to the response to shear of the semiflexible filaments forming at low temperature via hydrogen bonding and alpha-helix formation (64); however, the value of K' was significantly smaller than for EKGel at 10 °C.

We conclude that EKGel recapitulates the behavior of biological fibrous networks by exhibiting stiffening at low strains. Notably, while some nonfibrillar, flexible-strand gels formed by cross-linked polymer molecules can exhibit strain-stiffening behavior at high cross-linking density (64, 65), they only do so at γ_c values in the range of 1.0 to 4.0, well above the range of γ_c from 0.11 to 0.18 observed for EKGel in our work.

Interestingly, EKGel with different compositions exhibited a characteristic rate of stress-stiffening above the critical shear stress σ_c, determined by scaling of K' with σ. Fig. 5 shows that when normalizing K' by G, and σ by σ_c and γ by γ_c, based on the results shown in Fig. 4 and *SI Appendix*, Fig. S8, the dependence of K' vs. σ and γ in the strain-stiffening regime for EKGels with all compositions falls onto a single curve. This dependence was in agreement with theoretical prediction of the variation in K'/G vs. σ/σ_c (*SI Appendix*, Eqs. **S26** and **S29**). Similarly, when normalizing γ by γ_c the dependence of K'/G vs. γ/γ_c (*SI Appendix*, Eqs. **S25** and **S28**) in the strain-stiffening regime for EKGel with all compositions fell onto a single curve (Fig. 5*B*).

Earlier works have simulated two-dimensional networks of straight filaments that were originally thermally equilibrated and subsequently quenched in the bent state (12). In these simulations, the authors observed a transition from bending- to stretching-mediated elasticity, similar to the strain-stiffening cross-over observed in the present work (Fig. 5). The developed analytical theory (presented in detail in *SI Appendix*) is also consistent with these numerical studies, as well as with the predicted delay of the bending-to-stretching transition with increasing filament bending (12).

To examine the reversibility of nonlinear EKGel strain-stiffening, hydrogels with C_{total}= 1.0 to 5.0 wt% (C_{aCNC}/C_{gel} = 1.0) was subjected to a cyclic amplitude sweep experiment. *SI Appendix*, Fig. S11 *A*–*C* shows the time dependence of K' over several cycles for with C_{total} in the range of 1.0 to 5.0 wt%, when the value of σ was gradually increased from 1.0 to 60 Pa, and subsequently, decreased to 1.0 Pa. *SI Appendix*, Fig. S11*D* shows the cyclic amplitude sweep of K', plotted as a function of σ. The results of several cycles were highly reproducible and were superimposed, including the value of σ_c, with no observable hysteresis.

As discussed above, a second characteristic feature of fibrous networks such as fibrin, collagen, platelet-poor plasma, and polyisocyanopeptide gels is their asymmetric mechanical response: they strongly stiffen in response to shear or extensional strain, but weakly soften when compressed (18–20). Compression leads to fiber bending and buckling, with buckled fibers not contributing to the network stiffness, so that as compressive strain increases,

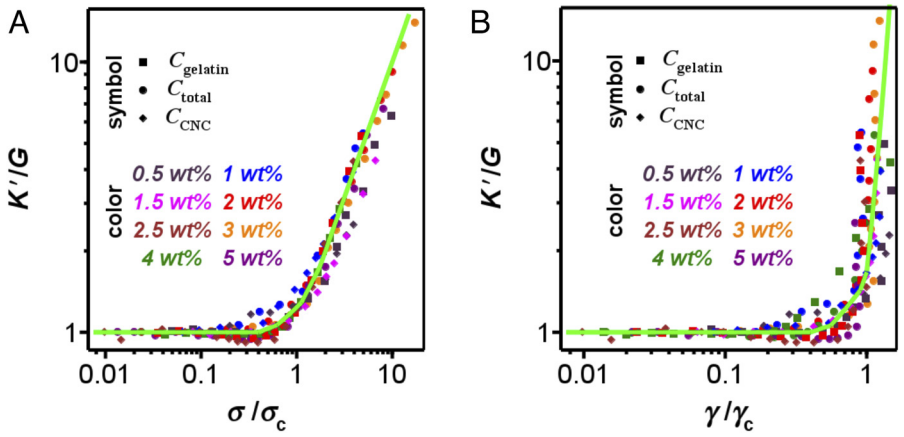

Fig. 5. Strain-stiffening of EKGel with different compositions. (*A*) "Universal" dependence of normalized differential modulus K'/G on normalized shear stress σ/σ_c for EKGel with different compositions. The solid green line shows theoretical prediction of the variation in K'/G vs. σ/σ_c. (*SI Appendix*, Eqs. **S26** and **S29**). (*B*) Universal dependence of normalized differential modulus K'/G on normalized shear strain γ/γ_c for EKGel with different compositions. The solid green line shows theoretical prediction of the variation in K'/G vs. γ/γ_c described by (*SI Appendix*, Eqs. **S25** and **S28**). All results are shown at 37 °C. The maximal stress corresponds to the highest stress measured before hydrogel rupture. The initial shear stress was 1 Pa.

fibrillar networks soften. In contrast, extension stretches individual fibers, resulting in gel stiffening (14).

To investigate the mechanical asymmetry of EKGel we measured its storage modulus, G', upon oscillatory shear in x-y plane at a varying axial strain in z-direction (that is, by subjecting EKGel to compression and expansion). An EKGel was formed between two plates of an oscillatory shear rheometer (Fig. 6*A*). Mineral oil was added to the edge of the hydrogel to prevent the loss of water upon hydrogel drying. Gelation was confirmed when the shear storage modulus, G', of EKGel reached a plateau. To induce different axial strains, the gap between the two plates was changed as $\varepsilon_z = (h - h_i)/h_i$, where h and h_i are the gap height at the point of G' measurement and initial gap height, respectively. In this experimental design, $\varepsilon_z = 0$ corresponds to the undeformed EKGel, $\varepsilon_z < 0$ to the compressed EKGel, and $\varepsilon_z > 0$ to gel stretching while it adheres to the parallel plates (Fig. 1) (18). The value of G' was determined at 1% oscillatory shear strain and a frequency of 1 Hz (within the linear regime, *SI Appendix*, Fig. S12), with EKGel being equilibrated for 1 min at each axial strain. To confirm that this observation was not a result of the poroelastic effect, we monitored the change in normal stress (N) and G' as function of time at $\varepsilon_z = -0.1$ and $+0.1$ (*SI Appendix*, Fig. S13). While the value of N did not relax to the equilibrium value within 1 min, the variation of G' reached close-to-equilibrium value after 1 min. *SI Appendix*, Fig. S13 also shows that the mechanical asymmetry of EKGel did not significantly change when EKGel equilibration time was increased to 10 min. We therefore conclude that the results in Fig. 6 do not originate primarily from the poroelastic effect.

Fig. 6*B* shows that upon EKGel compression, with strain ε_z changing from 0 to −0.1, the value of G' gradually decreased to 15% of its original value. In contrast, when stretching EKGel from $\varepsilon_z = 0$ to $+0.1$, the value of G' increased by 46%. For comparison, Fig. 6*B* shows the dependence of G' vs. ε_z for a fibrin gel, for which softening under compression and stiffening when stretched have been reported (18, 19). In our work, when fibrin gel was compressed from $\varepsilon_z = 0$ to −0.1, the value of G' gradually decreased to 20% of its original value, while upon its stretching from $\varepsilon_z = 0$ to $+0.1$, the value of G' increased by 200%. Thus, in addition to mimicking nonlinear strain-stiffening, the mechanical asymmetry of biological fibrous gels was recapitulated in EKGel, although the degree of stiffening upon extension was lower by a factor of four in EKGel. In contrast to fibrin gel and EKGel, upon compression of flexible network polyacrylamide from $\varepsilon_z = 0$ to −0.1, the value of G' steadily increased by 19% (Fig. 6*B*). These results again highlight the biomimetic mechanical response to compression of EKGel, which is distinct from the response of synthetic hydrogels formed by flexible molecules.

Compression-induced softening of EKGel was reproduced in the repeated compression-decompression cycles. Fig. 6*C* shows the variation in G' vs. ε_z in three cycles, with compression changing from $\varepsilon_z = 0$ to $\varepsilon_z = -0.1$, followed by extension from $\varepsilon_z = 0$ to $\varepsilon_z = +0.1$. Consistently, EKGel weakly softened during compression and strongly stiffened during extension. This result indicated that compression-induced softening cannot be attributed to the irreversible damage of the fibers or network. *SI Appendix*, Fig. S14 shows superimposed plots of the variation in G' and ε_z over three consecutive compression/extension cycles. *SI Appendix*, Fig. S15 shows the reproducibility of the mechanical asymmetry behavior for EKGel.

Next, we investigated the dependence of EKGel's mechanical asymmetry on its composition. Fig. 6*D* shows the dependence of G' vs. ε_z for EKGel with $1.0 \le C_{total} \le 5.0$ wt% at $C_{aCNC}/C_{gel} = 1.0$. For EKGel with all compositions studied, softening occurred upon compression (reducing ε_z from 0 to −0.1) and stiffening occured upon extension (increasing ε_z from 0 to +0.1) (Fig. 6*D*). When $G'(\varepsilon_z)$ was normalized with respect to $G'(\varepsilon_z = 0)$, the relative degrees of compression-softening and stress-stiffening were similar (Fig. 6*E*). This dependence was in agreement with theoretically predicted variation of the normalized G' vs. ε_z, determined by *SI Appendix*, Eqs. **S35** and **S37** and shown by the solid black line in Fig. 6*E*.

Discussion

We explored the structural characteristics and mechanical properties of an engineered fibrous hydrogel (EKGel) and showed that it displays both nonlinear strain-stiffening and mechanical asymmetry. We demonstrate that EKGel's elasticity is of enthalpic origin, similar to biological fibrous networks of e.g., fibrin and collagen, and conclude that the nonlinear mechanical properties of EKGel originate from the asymmetry in bending and stretching stiffness of the constituent filaments of the gel.

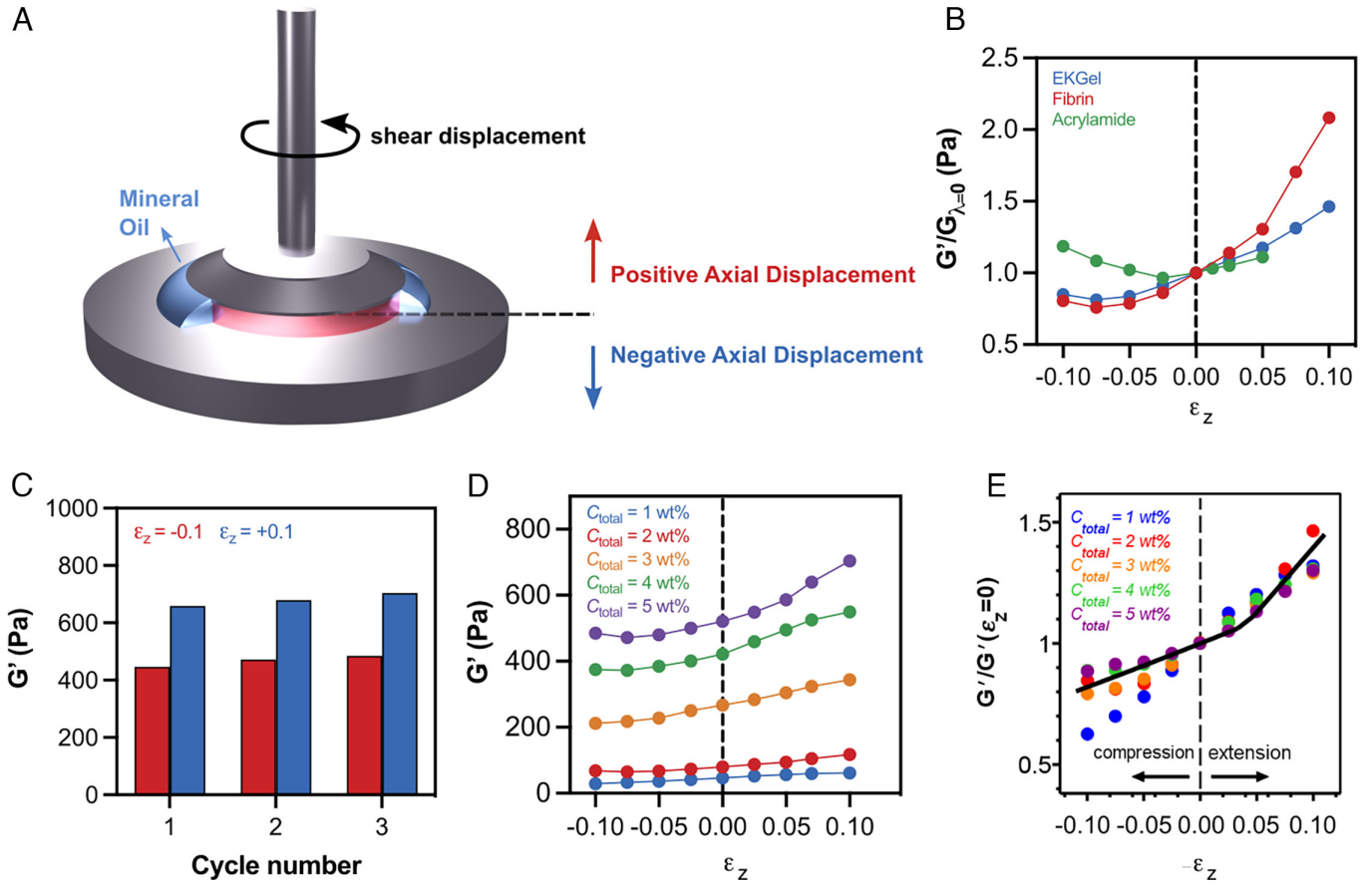

Fig. 6. Mechanical asymmetry of EKGel. (*A*) Experimental design for measurements of mechanical anisotropy of hydrogels. Axial strain (ε_z) was adjusted by changing the gap between the rheometer plates, with $\varepsilon_z = 0$ being defined as the initial EKGel thickness. (*B*) Variation of G' vs. ε_z for EKGel with C_{total} = 2.0 wt% (C_{aCNC}/C_{gel} = 1.0), polyacrylamide (acrylamide and the *bis*-acrylamide concentrations were 3.0 and 0.079 wt%, respectively), and fibrin (bovine fibrin and thrombin concentrations were 22.8 mg/mL and 5 U/mL, respectively, in tris-buffered saline with 3 mM $CaCl_2$). The solid lines are given for eye guidance. (*C*) Reversibility of compression-softening and stretch-stiffening for EKGel with C_{total}= 5.0 wt% (C_{aCNC}/C_{gel} = 1.0) over three cycles of increasing ε_z from −0.1to + 0.1. (*D*) Dependence of G' on ε_z for EKGel with different C_{total} (C_{aCNC}/C_{gel} = 1.0). Colored lines are added for eye guidance. (*E*) Variation of G' normalized to G' at $\varepsilon_z = 0$, plotted as a function of ε_z for EKGel with different C_{total} (C_{aCNC}/C_{gel} = 1.0). The solid black line in (*E*) shows theoretically predicted dependence of the normalized G' vs. ε_z, determined from *SI Appendix*, Eqs. **S35** and **S37**.

We introduced a theoretical framework to describe the mechanical asymmetry of enthalpic filamentous networks. The affine theoretical model was applied to predict the nonlinear properties of EKGel, based on the strong force-extension asymmetry of the constituent athermal filaments with $k_s/k_b \gg 1$. The results of the theoretical prediction of strain-stiffening and compression/stretching-mediated asymmetric change of the shear modulus of EKGel were in agreement with experimental observations. This theoretical framework can serve as a foundation for research on nonlinear mechanical properties of other enthalpic fibrous hydrogels.

The described hydrogel was formed by composite fibers, which offers flexibility in the modulation of the hydrogel chemistry, structure, and properties. The variation in the hydrogel composition led to a broad range of shear modulus; however, the onsets of nonlinear mechanical properties, that is, the dependences of K'/G vs. σ/σ_c and K''/G vs. γ/γ_c were consistent for EKGel's with different compositions. These results suggest that nonlinear mechanical properties are general for networks formed by long filaments that are substantially stiffer upon stretching and softer upon bending. In contrast, we show that in the range of stresses and strains studied, a hydrogel formed by the cross-linked polyacrylamide (a molecular gel) does not exhibit a nonlinear mechanical behavior. Studies of other mechanical properties of EKGel's enthalpic network, including its fracture behavior, are the subject of future research.

The described EKGel is an example of a filamentous hydrogel prepared from high-aspect ratio nanocolloidal building blocks. Our approach can be used for the preparation of fibrous materials derived from other high aspect ratio rigid nanoparticles such as carbon nanotubes, inorganic nanorods, or chitosan nanowhiskers, which can open the door to the engineering of filamentous networks with functional (e.g., optical and electronic) properties and nonlinear mechanical properties. From the practical perspective, EKGel is prepared from two cost-effective, biosourced components. It does not require a complex synthetic procedure, and gel formation process is simple and robust. Thus, our material is accessible to a broad scientific community.

We note that while nonlinear mechanical properties of fibrous hydrogels formed by bottlebrush (41, 42) and polyisocyanopeptide (43, 44) polymers have been reported, fibers in EKGel are made from the composite material, that is, rod-like nanoparticles and a polymer. This additional complexity provides an additional ability of fine-tuning hydrogel's properties, e.g., by changing the degree of cross-linking of the polymer in the fibers, by varying the number of binding sites of the polymer to the nanoparticles, or by using a conductive polymer.

The ability to alter and understand the mechanical properties of engineered filamentous hydrogels can be used to facilitate their applications in mechanobiology. There has been significant past work with flexible-strand hydrogels to establish that matrix

stiffness impacts different biological processes, including drug response, stem-cell differentiation, and the progression of cancer and fibrosis (66–68). Importantly, the conclusions were made by using hydrogel matrixes that did not recapitulate the filamentous architecture or nonlinear mechanical properties of the native ECM. Studies of the impact of matrix stiffness have to be performed with biomimetic hydrogels such as EKGel to verify the results of previous studies. Furthermore, while the fibrillar networks that make up the ECM and cytoskeleton display both nonlinear strain-stiffening and mechanical asymmetry, the biological impact of these properties remains understudied.

Finally, given EKGel's biocompatibility with different types of cells (45–47, 54), this hydrogel can serve as a platform for mechanobiology studies to elucidate the impact of nonlinear mechanics on biological processes. Its biocompatibility, biomimetic fibrillar architecture, cost-effectiveness, and tunable strain-stiffening make it a promising material for this purpose.

Conclusions

In summary, we show that an engineered covalently cross-linked fibrous hydrogel derived from cellulose nanocrystals and gelatin exhibits nonlinear shear-stiffening and compression-induced softening, thus, recapitulating the mechanical behavior of biological gels. The variation in gel composition enabled a broad-range variation in its mechanical properties, while the nonlinear mechanical properties were observed acroos for hydrogels with different compositions. We show that this gel belongs to the athermal bent class of fibrous networks, in agreement with an affine model. Further steps should exploit the composite nature of the hydrogel fibers formed by nanoparticles and a polymer to expand the range of mechanical properties or achieve additional functionality, e.g., conductivity of the gel. On the other hand, owing to its biocompatibility, biomimetic fibrous architecture, and cost-effectiveness, this gel would serve as a promising material for studies of the impact of nonlinear mechanical properties on cell behavior.

Materials and Methods

Materials. Type A gelatin from porcine skin (300 g bloom, cat. #G1890), ethylene glycol (cat. #102466), 25 % glutaraldehyde aqueous solution (cat. #354400), fibrinogen from bovine plasma (F8630), tris buffered saline (cat. #T5030), anhydrous calcium chloride (cat. #C1016), thrombin from bovine plasma (cat. #T4648), cellulose membrane dialysis tubing (12 kDa cutoff, cat. #D9277-100FT), and sodium periodate (cat. # 311448) were purchased from Sigma-Aldrich. Both 1X and 10X formulations of Hanks Balanced Salt Solution (GIBCO) were purchased from Fisher Scientific, Canada (1X Cat. #15266355, 10X: Cat. #11530466). Collagen-I was extracted from rat-tail tendons (69). Matrigel was purchased from Corning (cat. #356234). Cellulose nanocrystals were purchased as an aqueous 12.2 wt% suspension from the University of Maine Process Development. All chemicals were used as received without further purification unless otherwise specified.

Preparation of aCNCs. Sodium periodate oxidation was used to introduce aldehyde groups onto the CNC surface using a previously reported method (35, 46). For oxidation, 1.2 g of sodium periodate was added to 200 mL of a 1 wt% aqueous suspension of CNCs in a 500 mL round bottom flask. The suspension was covered with tin foil to prevent photodecomposition of sodium periodate and stirred for 2 h at room temperature. Ethylene glycol (600 μL) was then added to quench the reaction. The suspension was then dialyzed against miliQ grade deionized water (12 kDa molecular weight cutoff, 10 changes). The suspension was concentrated to >3 wt% under rotary evaporation.

Gelation of EKGel. EKGel was prepared from three precursor solutions: aCNC in HBSS, gelatin in HBSS, and HBSS buffer. The aCNC suspension was prepared by adding 10X HBSS buffer to give a final concentration of 1X HBSS (250 μL 10X HBSS in 2.25 mL aCNC). Gelatin was prepared by dissolving powdered gelatin in 1X HBSS to give a final gelatin concentration of 10 wt%. The precursor solutions were added in a specific ratio to give the desired C_{total}, C_{aCNC}, and C_{gel}. The order of addition was as follows: 1) HBSS, 2) aCNCs, and 3) gelatin, with vortexing between each addition to ensure that the hydrogel was homogenous. The hydrogel is incubated at 37 °C for gelation.

Confocal Microscopy of EKGel. To visualize the location of gelatin and aCNCs within the EKGel, we covalently labeled gelatin with rhodamine-B-isothiocyanate (RBITC) and the aCNCs with CF-488A hydrazide® (Sigma Aldrich) as described below. EKGel was prepared as described above, but aCNCs were replaced with CF-488A-labeled aCNCs, and gelatin was replaced with RBITC-labeled gelatin. Immediately after mixing, a droplet of the EKGel precursor suspension was placed on a glass slide and covered with a glass coverslip (#1.5 thickness). The samples were sealed with nail polish and incubated overnight at 37 °C to allow for complete gelation. The fluorescent EKGel samples were imaged using a Nikon AR1 confocal microscope with a 100× oil immersion lens. To image CF-488A-labeled aCNCs, a 488-nm laser was used; a 561-nm laser was used to image RBITC-labeled gelatin. The Pearson colocalization coefficient (PCC) was determined using ImageJ software.

Quantifying the Density of Aldehyde Groups on CNCs. To characterize the extent of CNC functionalization, the aldehyde groups were converted to oxime groups with hydroxylamine hydrochloride (55, 56). An aCNC suspension was prepared by suspending 100 mg of aCNCs in 30 mL of deionized water. A hydroxylamine hydrochloride solution was prepared by dissolving 0.43 g of hydroxylamine hydrochloride in 20 mL of deionized water. The pH of the aCNC suspension and the hydroxylamine hydrochloride solution was adjusted to 4.5. Subsequently, the aCNC suspension and the hydroxylamine hydrochloride solution were mixed and stirred at room temperature for 24 h. The conversion of aldehyde groups to oxime groups with hydroxylamine hydrochloride resulted in the formation of HCl. The density of aldehyde groups was calculated by titrating the HCl with 0.1 M NaOH using a pH meter (EcoMet P25).

Quantifying the Number of Imine Cross-Links. The concentration of imine cross-links in EKGel was determined by using the TNBS assay, which quantifies the concentration of amine groups in the hydrogel that have not been consumed by cross-linking with CNCs, that is, free amine groups (70). We determined the concentration of free amine groups in EKGel with different compositions. The concentration of imine cross-links in EKGels was then determined by subtracting the number of free amine groups in the hydrogel from the number of free amine groups in the precursor gelatin solution. More specifically, EKGels with different compositions and gelatin solutions with varying concentrations were prepared in a 96-well plate (50 μL per well) and allowed to gel overnight at 37 °C. Next, 100 μL of 0.5 w/v% TNBS in 0.1 M sodium carbonate buffer (pH 9) was added to each well. After incubating the samples at 37 °C for 2 h, their absorbance at λ = 500 nm was determined using a CLARIOstar plate reader. To account for the differences in light scattering by EKGels with different C_{aCNC}, the corresponding TNBS-free hydrogels were used as reference samples for background subtraction. To determine the concentration of amine groups in EKGel, we used a calibration curve that was constructed using glycine standard solutions.

SEM Imaging of EKGel. The structure of EKGel was studied by using SEM. Supercritical point drying was utilized to prepare hydrogel samples. EKGel samples were allowed to gel overnight at 37 °C and then were fixed by submerging them in 2 wt% glutaraldehyde in HBSS for 24 h and washed with deionized water three times. Subsequently, the water was exchanged with ethanol by consecutively submerging the EKGel for 30 min in 30, 50, 70, and 90 v/v% ethanol/water mixtures and then finally in anhydrous ethanol three times. Ethanol was then removed using an Autosamdri-810 Tousimis critical point dryer. The dried EKGel was then fractured. The samples were imaged on a Quanta FEI Scanning Electron Microscope (10 kV). For enhanced visualization, the samples were gold-coated using an SC7640 High Resolution Sputter Coater (Quorum Technologies). The analysis of fiber diameter was performed on EKGel samples without gold sputtering, as the fiber dimensions could be obscured by gold coating. Structural analysis was performed manually using ImageJ software. One EKGel sample was imaged for each C_{total}. To avoid bias, the image analysis was conducted independently by two scientists. For each EKGel sample, 6 to 10 images of different regions were taken, and 10 to 20 fibers were analyzed in each image.

Rheology. The rheological properties of the EKGel were characterized at 37 °C using a DHR-1 Rheometer (TA Instruments) with a cone and plate geometry, with a cone angle and diameter of 0.9675° and 40 mm, respectively. An integrated Peltier Plate was used to control the temperature, and a mineral oil was added around the edge of the cone to prevent solvent evaporation. To add the gel in the rheometer, gel precursors were mixed and pipetted onto the Peltier plate. The cone was lowered to the geometry gap, and the gel precursors were dispersed by rotating the cone. Even dispersion of the precursors was visually confirmed. The hydrogel precursors were equilibrated at 37 °C for 5 h before experiments to ensure gelation. Unless otherwise specified, one sample of EKGel was characterized for each hydrogel composition and temperature.

To determine the differential modulus, K', in nonlinear strain stiffening experiments, we used a prestress protocol, in which the gel was subjected to prestress (σ) ranging from 0.5 to 1,000 Pa and subsequently, applied small oscillatory stresses that are <10% of the applied prestress (43, 61). The value of σ_c was determined by extrapolating the variation of K' vs. σ in the high stress region to $K'/G = 1.0$. This point was found by extrapolating log K'/G vs. log σ to log $K'/G = 0$ with nonlinear regression analysis, which corresponds to log σ_c. The critical strain was found as $\gamma_c = \sigma_c / G$.

To determine the stiffness of EKGel under compression or extension, we determined the storage modulus (G') at different axial strains. The storage modulus was measured at 1 wt% oscillatory shear strain and a frequency of 1 Hz, using parallel plates with a diameter of 40 mm. The initial gap between the plates was 400 μm. The gap was adjusted to change the axial strain from ±10% (360 to 440 μm), and the hydrogels were allowed to equilibrate for 1 min at each axial strain.

Data, Materials, and Software Availability. All data needed to evaluate the conclusions in the paper are included in the article and/or *SI Appendix*. Replication data for gel structural and mechanical property analysis is deposited on Borealis (https://doi.org/10.5683/SP3/4GZS1X) (71).

ACKNOWLEDGMENTS. E.K. thanks the Canada Research Chairs Program. E.P. is grateful to NSERC for the Canada Graduate Scholarship–Doctoral Program. M.R. acknowledges financial support from the NSF under Grant EFMA-1830957 and the NIH under Grant P01-HL164320.

Author affiliations: [a]Department of Chemistry, University of Toronto, Toronto, ON M5S3H6, Canada; [b]Department of Chemical Engineering, University of Waterloo, Waterloo, ON N2L3G1, Canada; [c]Waterloo Institute for Nanotechnology, University of Waterloo, Waterloo, ON N2L3G1, Canada; [d]N. E. Bauman Moscow State Technical University, Moscow 105005, Russia; [e]Department of Applied Oral Sciences, Faculty of Dentistry, Dalhousie University, Halifax, NS B3H4R2, Canada; [f]Center of Soft Matter and Physics of Fluids, P. N. Lebedev Physics Institute, Russian Academy of Sciences, Moscow 117924, Russia; [g]Department of Theoretical Physics, Moscow Institute of Physics and Technology, Moscow 141700, Russia; [h]Department of Mechanical Engineering and Materials Science, Duke University, Durham, NC 27708; [i]Department of Biomedical Engineering, Duke University, Durham, NC 27708; [j]Department of Physics, Duke University, Durham, NC 27708; [k]Department of Chemistry, Duke University, Durham, NC 27708; [l]Institute for Chemical Reaction Design and Discovery, Hokkaido University, Sapporo 001-0021, Japan; [m]Institute of Biomedical Engineering, University of Toronto, Toronto, ON M5S3G9, Canada; and [n]Department of Chemical Engineering and Applied Chemistry, University of Toronto, Toronto, ON M5S3E5, Canada

Author contributions: E.P. and E.K. designed research; E.P., S.M., Z.C., V.A., I.Y., S.P., and M.R. performed research; E.P. and S.M. analyzed data; and E.P., S.P., M.R., and E.K. wrote the paper.

1. M. Schliwa, *The Cytoskeleton* (Springer, 2012).
2. F. T. Bosman, I. Stamenkovic, Functional structure and composition of the extracellular matrix. *J. Pathol.* **200**, 423–428 (2003).
3. A. E. X. Brown, R. I. Litvinov, D. E. Discher, P. K. Purohit, J. W. Weisel, Multiscale mechanics of fibrin polymer: Gel stretching with protein unfolding and loss of water. *Science* **325**, 741–744 (2009).
4. R. S. Sopher *et al.*, Nonlinear elasticity of the ECM fibers facilitates efficient intercellular communication. *Biophys. J.* **115**, 1357–1370 (2018).
5. B. R. Seo *et al.*, Collagen microarchitecture mechanically controls myofibroblast differentiation. *Proc. Natl. Acad. Sci. U.S.A.* **117**, 11387–11398 (2020).
6. M. S. Hall *et al.*, Fibrous nonlinear elasticity enables positive mechanical feedback between cells and ECMs. *Proc. Natl. Acad. Sci. U.S.A.* **113**, 14043–14048 (2016).
7. K. Liu, M. Wiendels, H. Yuan, C. Ruan, P. H. J. Kouwer, Cell-matrix reciprocity in 3D culture models with nonlinear elasticity. *Bioact. Mater.* **9**, 316–331 (2022).
8. C. Storm, J. J. Pastore, F. C. MacKintosh, T. C. Lubensky, P. A. Janmey, Nonlinear elasticity in biological gels. *Nature* **435**, 191–194 (2005).
9. M. L. Gardel *et al.*, Elastic behavior of cross-linked and bundled actin networks. *Science* **304**, 1301–1305 (2004).
10. Y.-C. Lin *et al.*, Origins of elasticity in intermediate filament networks. *Phys. Rev. Lett.* **104**, 058101 (2010).
11. N. Y. Yao *et al.*, Elasticity in ionically cross-linked neurofilament networks. *Biophys. J.* **98**, 2147–2153 (2010).
12. P. R. Onck, T. Koeman, T. van Dillen, E. van der Giessen, Alternative explanation of stiffening in cross-linked semiflexible networks. *Phys. Rev. Lett.* **95**, 178102 (2005).
13. J. V. Shah, P. A. Janmey, Strain hardening of fibrin gels and plasma clots. *Rheol. Acta* **36**, 262–268 (1997).
14. R. E. Shadwick, Mechanical design in arteries. *J. Exp. Biol.* **202**, 3305–3313 (1999).
15. J. Notbohm, A. Lesman, P. Rosakis, D. A. Tirrell, G. Ravichandran, Microbuckling of fibrin provides a mechanism for cell mechanosensing. *J. R. Soc. Interf.* **12**, 20150320 (2015).
16. J. P. Winer, S. Oake, P. A. Janmey, Non-linear elasticity of extracellular matrices enables contractile cells to communicate local position and orientation. *PLoS One* **4**, e6382 (2009).
17. M. Aghvami, K. L. Billiar, E. A. Sander, Fiber network models predict enhanced cell mechanosensing on fibrous gels. *J. Biomech. Eng.* **138**, 1010061–10100611 (2016).
18. A. S. G. van Oosten *et al.*, Uncoupling shear and uniaxial elastic moduli of semiflexible biopolymer networks: Compression-softening and stretch-stiffening. *Sci. Rep.* **6**, 19270 (2016).
19. M. Vahabi *et al.*, Elasticity of fibrous networks under uniaxial prestress. *Soft Matter* **12**, 5050–5060 (2016).
20. P. Almeida, P. A. Janmey, P. H. J. Kouwer, Fibrous hydrogels under multi-axial deformation: Persistence length as the main determinant of compression softening. *Adv. Funct. Mater.* **31**, 2010527 (2021).
21. M. Kalli, T. Stylianopoulos, Defining the role of solid stress and matrix stiffness in cancer cell proliferation and metastasis. *Front. Oncol.* **8**, 55 (2018).
22. A. J. Licup *et al.*, Stress controls the mechanics of collagen networks. *Proc. Natl. Acad. Sci. U.S.A.* **112**, 9573–9578 (2015).
23. S. Münster *et al.*, Strain history dependence of the nonlinear stress response of fibrin and collagen networks. *Proc. Natl. Acad. Sci. U.S.A.* **110**, 12197–12202 (2013).
24. O. V. Kim, R. I. Litvinov, J. W. Weisel, M. S. Alber, Structural basis for the nonlinear mechanics of fibrin networks under compression. *Biomaterials* **35**, 6739–6749 (2014).
25. D. Vader, A. Kabla, D. Weitz, L. Mahadevan, Strain-induced alignment in collagen gels. *PLoS ONE* **4**, e5902 (2009).
26. L. Martikainen, K. Bertula, M. Turunen, O. Ikkala, Strain stiffening and negative normal force of agarose hydrogels. *Macromolecules* **53**, 9983–9992 (2020).
27. H. Kamata, Y. Akagi, Y. Kayasuga-Kariya, U.-I. Chung, T. Sakai, 'Nonswellable' hydrogel without mechanical hysteresis. *Science* **343**, 873–875 (2014).
28. S. Kondo *et al.*, Reliable hydrogel with mechanical 'fuse link' in an aqueous environment. *Adv. Mater.* **27**, 7407–7411 (2015).
29. K. Hayashi *et al.*, Fast-forming hydrogel with ultralow polymeric content as an artificial vitreous body. *Nat. Biomed. Eng.* **1**, 0044 (2017).
30. D. E. Apostolides, T. Sakai, C. S. Patrickios, Dynamic covalent star poly(ethylene glycol) model hydrogels: A new platform for mechanically robust, multifunctional materials. *Macromolecules* **50**, 2155–2164 (2017).
31. M. P. Lutolf, J. A. Hubbell, Synthetic biomaterials as instructive extracellular microenvironments for morphogenesis in tissue engineering. *Nat. Biotechnol.* **23**, 47–55 (2005).
32. E. Prince, E. Kumacheva, Design and applications of man-made biomimetic fibrillar hydrogels. *Nat. Rev. Mater.* **4**, 99–115 (2019).
33. M. Chau *et al.*, Composite hydrogels with tunable anisotropic morphologies and mechanical properties. *Chem. Mater.* **28**, 3406–3415 (2016).
34. M. Chau *et al.*, Ion-mediated gelation of aqueous suspensions of cellulose nanocrystals. *Biomacromolecules* **16**, 2455–2462 (2015).
35. E. Prince *et al.*, Patterning of structurally anisotropic composite hydrogel sheets. *Biomacromolecules* **19**, 1276–1284 (2018).
36. Y. Li *et al.*, Supramolecular nanofibrillar thermoreversible hydrogel for growth and release of cancer spheroids. *Angew. Chem. Int. Ed Engl.* **56**, 6083–6087 (2017).
37. J. C. Stendahl, M. S. Rao, M. O. Guler, S. I. Stupp, Intermolecular forces in the self-assembly of peptide amphiphile nanofibers. *Adv. Funct. Mater.* **16**, 499–508 (2006).
38. R. N. Shah *et al.*, Supramolecular design of self-assembling nanofibers for cartilage regeneration. *Proc. Natl. Acad. Sci. U.S.A.* **107**, 3293–3298 (2010).
39. K. Bertal *et al.*, Antimicrobial activity of novel biocompatible wound dressings based on triblock copolymer hydrogels. *J. Mater. Sci.* **44**, 6233–6246 (2009).
40. J. Madsen *et al.*, Biocompatible wound dressings based on chemically degradable triblock copolymer hydrogels. *Biomacromolecules* **9**, 2265–2275 (2008).
41. M. Vatankhah-Varnosfaderani *et al.*, Chameleon-like elastomers with molecularly encoded strain-adaptive stiffening and coloration. *Science* **359**, 1509–1513 (2018).
42. F. Vashahi *et al.*, Injectable bottlebrush hydrogels with tissue-mimetic mechanical properties. *Sci. Adv.* **8**, eabm2469 (2022).
43. P. H. J. Kouwer *et al.*, Responsive biomimetic networks from polyisocyanopeptide hydrogels. *Nature* **493**, 651–655 (2013).
44. M. Jaspers *et al.*, Ultra-responsive soft matter from strain-stiffening hydrogels. *Nat. Commun.* **5**, 5808 (2014).
45. E. Prince *et al.*, Biomimetic hydrogel supports initiation and growth of patient-derived breast tumor organoids. *Nat. Commun.* **13**, 1466 (2022).
46. E. Prince, Z. Chen, N. Khuu, E. Kumacheva, Nanofibrillar hydrogel recapitulates changes occurring in the fibrotic extracellular matrix. *Biomacromolecules* **22**, 2353–2362 (2021).
47. E. Prince *et al.*, Microfluidic arrays of breast tumor spheroids for drug screening and personalized cancer therapies. *Adv. Healthc. Mater.* **11**, e2101085 (2021).
48. Y. Li *et al.*, Fibrous hydrogels under biaxial confinement. *Nat. Commun.* **13**, 3264 (2022).
49. A. J. Licup, A. Sharma, F. C. MacKintosh, Elastic regimes of subisostatic athermal fiber networks. *Phys. Rev. E.* **93**, 012407 (2016).
50. K. A. Jansen *et al.*, The role of network architecture in collagen mechanics. *Biophys. J.* **114**, 2665–2678 (2018).
51. S. B. Ross-Murphy, Structure and rheology of gelatin gels: Recent progress. *Polymer (Guildf.)* **33**, 2622–2627 (1992).

52. H. B. Bohidar, Hydrodynamic properties of gelatin in dilute solutions. *Int. J. Biol. Macromol.* **23**, 1–6 (1998).
53. Z. Chen *et al.*, Microfluidic arrays of dermal spheroids: A screening platform for active ingredients of skincare products. *Lab Chip.* **21**, 3952–3962 (2021).
54. K. W. Dunn, M. M. Kamocka, J. H. McDonald, A practical guide to evaluating colocalization in biological microscopy. *Am. J. Physiol. Cell Physiol.* **300**, C723–C742 (2011).
55. Q. X. Hou, W. Liu, Z. H. Liu, L. L. Bai, Characteristics of wood cellulose fibers treated with periodate and bisulfite. *Ind. Eng. Chem. Res.* **46**, 7830–7837 (2007).
56. U.-J. Kim, M. Wada, S. Kuga, Solubilization of dialdehyde cellulose by hot water. *Carbohydr. Polym.* **56**, 7–10 (2004).
57. P. G. De Gennes, Dynamics of entangled polymer solutions. II. Inclusion of hydrodynamic interactions. *Macromolecules* **9**, 594–598 (1976).
58. C. F. Schmidt, M. Baermann, G. Isenberg, E. Sackmann, Chain dynamics, mesh size, and diffusive transport in networks of polymerized actin: A quasielastic light scattering and microfluorescence study. *Macromolecules* **22**, 3638–3649 (1989).
59. P. G. De Gennes, P. Pincus, R. M. Velasco, F. Brochard, Remarks on polyelectrolyte conformation. *J. Phys.* **37**, 1461–1473 (1976).
60. N. Y. Yao *et al.*, Characterizing the non-linear rheology of biopolymer networks using inertio-elastic oscillations. *AIP Conf Proc* **1027**, 621–623 (2008).
61. M. Djabourov, J. Leblond, P. Papon, Gelation of aqueous gelatin solutions. I. Structural investigation. *J. Phys.* **49**, 319–332 (1988).
62. N. Gasek, D. J. Weiss, Effect of temperature on gelation and cross-linking of gelatin methacryloyl for biomedical applications. *Phys. Fluids (1994)* **32**, 033102 (2020).
63. Z. Yang *et al.*, Nonlinear behavior of gelatin networks reveals a hierarchical structure. *Biomacromolecules* **17**, 590–600 (2016).
64. K. A. Erk, K. J. Henderson, K. R. Shull, Strain stiffening in synthetic and biopolymer networks. *Biomacromolecules* **11**, 1358–1363 (2010).
65. B. Yan *et al.*, Duplicating dynamic strain-stiffening behavior and nanomechanics of biological tissues in a synthetic self-healing flexible network hydrogel. *ACS Nano* **11**, 11074–11081 (2017).
66. N. Gjorevski *et al.*, Designer matrices for intestinal stem cell and organoid culture. *Nature* **539**, 560–564 (2016).
67. A. J. Engler, S. Sen, H. L. Sweeney, D. E. Discher, Matrix elasticity directs stem cell lineage specification. *Cell* **126**, 677–689 (2006).
68. Y. S. Pek, A. C. A. Wan, J. Y. Ying, The effect of matrix stiffness on mesenchymal stem cell differentiation in a 3D thixotropic gel. *Biomaterials* **31**, 385–391 (2010).
69. N. Rajan, J. Habermehl, M.-F. Coté, C. J. Doillon, D. Mantovani, Preparation of ready-to-use, storable and reconstituted type I collagen from rat tail tendon for tissue engineering applications. *Nat. Protoc.* **1**, 2753–2758 (2006).
70. C. M. Ofner, Y. Zhang, V. C. Jobeck, B. J. Bowman, Crosslinking studies in gelatin capsules treated with formaldehyde and in capsules exposed to elevated temperature and humidity. *J. Pharm. Sci.* **90**, 79–88 (2001).
71. E. Prince, Replication data for "Nanocolloidal hydrogel mimics the structure and nonlinear mechanical properties of biological fibrous networks". Borealis. https://borealisdata.ca/dataset.xhtml?persistentId=doi:10.5683/SP3/4GZS1X. Deposited 23 November 2023.